2020 IEEE International Conference on Robotics and Automation (ICRA)
31 May - 31 August, 2020. Paris, France

Backlash-Compensated Active Disturbance Rejection Control of Nonlinear Multi-Input Series Elastic Actuators

Brayden DeBoon, Scott Nokleby, and Carlos Rossa

Abstract— **Series elastic actuators with passive compliance have been gaining increasing popularity in force-controlled robotic manipulators. One of the reasons is the actuator's ability to infer the applied torque by measuring the deflection of the elastic element as opposed to directly with dedicated torque sensors. Proper deflection control is pinnacle to achieve a desired output torque and, therefore, small deviances in positional measurements or a nonlinear deformation can have adverse effects on performance. In applications with larger torque requirements, the actuators typically use gear reductions which inherently result in mechanical backlash. This combined with the nonlinear behaviour of the elastic element and unmodelled dynamics, can severely compromise force fidelity.**

This paper proposes a backlash compensating active disturbance rejection controller (ADRC) for multi-input series elastic actuators. In addition to proper deflection control, a multi-input active disturbance rejection controller is derived and implemented experimentally to mitigate any unmodelled nonlinearities or perturbations to the plant model. The controller is experimentally validated on a hybrid motor-brake-clutch series elastic actuator and the controller performance is compared against traditional error-based controllers. It is shown that the backlash compensated ADRC outperforms classical PID and ADRC methods and is a viable solution to positional measurement error in elastic actuators.

I. Introduction

Series elastic actuators (SEAs) are becoming an elemental building block in many contemporary collaborative robotic systems. They introduce an elastic element between the mechanical drive and the robot arm making otherwise rigid structures compliant to contact with humans or other robots. Topologically, SEAs are more amenable to accurate force control than classical actuation techniques as the elastic element may be used to provide a direct force estimate. Certainly, the inherent advantages introduced by SEAs do not come without a cost. The nonlinear stiffness and potential backlash of the elastic element pose a challenging control issue in which classical force control methods may not be sufficient. The controller must satisfy its intended goal and control the output torque as efficiently as possible, while respecting the most important factor of human-machine interaction: the operator's safety. Any device working in close proximity to a human must hold this factor paramount.

Robotic systems interacting with humans typically contain a combination of hardware and software solutions to reduce the possibility of causing injury to the operators. On one hand, hardware solutions come in the form of series elasticity [1]–[4], compliant and/or flexible material [5]–[7], and push button killswitches. These solutions are physically implemented and cannot be changed without adapting the hardware. On the other hand, software solutions make use of sensors such as cameras, infrared sensors, motion sensors, laser rangefinders, and force/torque sensors to determine whether or not a human is operating near a robot [8], [9].

In order to improve torque control, torque range, bandwidth, and safety, SEAs are currently migrating to topologies that combine multiple active and passive devices embedded in the same actuator [3], [10]–[14]. More complex topologies introduce new challenges on their own. They usually come in the form of motors or brakes connected through a gearboxes, belts, harmonic drives, or cables. Unfortunately, this creates uncertainty in the form of backlash, that is, the tolerance in the physical meshing of gear teeth in a transmission system. Since SEAs use positional measurements to infer the torque experienced at the output, accurate torque control heavily relies on the controller's ability to compensate for concurrent nonlinear effects due to backlash and nonlinear compliance of the elastic element. Compensation techniques include dead zone functions [15], [16], exact models [17], describing functions, and hysteresis models [18].

The issue described above requires a controller that is robust enough to differentiate between perturbations caused by imperfect models and external inputs to the system [19]. Active disturbance rejection controllers (ADRC) mitigate this issue by encapsulating these perturbations into a common disturbance term which can be considered as a new state in the controller model. Typically, ADRC designed for SEA are single-input single-output systems (SISO) [20], [21]. In hybrid SEA topologies, it is common to have multiple control inputs that relate directly to the output torque [21], making SEAs multi-input multi-output (MIMO) systems.

Thus, besides nonlinearities and unmodelled dynamics, SEA controllers must also be able to handle multiple control inputs as opposed to classical single-input controllers reported in the literature [22]. For instance, the actuator proposed by the authors in [3] employs a brake and motor connected through a differential clutch (Fig. 2). As the motor compresses a torsion spring, the brake controls the amount of torque transferred from the spring to the end-effector hence improving force bandwidth and fidelity.

This paper proposes a unified torque controller for multi-input SEAs. The controller is based on an active disturbance rejection control architecture that has been combined with a backlash compensation model. The nonlinear behaviour of the SEA's spring constant, unmodelled dynamics, and

B. DeBoon, S. Nokleby, and C. Rossa (corresponding author) are with the Faculty of Engineering and Applied Science, Ontario Tech University, Oshawa, Ontario, Canada. E-mail: brayden.deboon@ontariotechu.net; scott.nokleby@ontariotechu.ca; carlos.rossa@ontariotechu.ca.

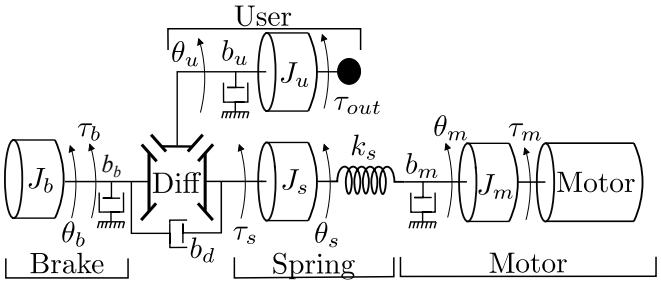

Fig. 1. Topology of a multi-input series elastic actuator from [3]. The actuator utilizes the properties of a differential gearbox to encompass various operating modes of elastic actuators. The series elasticity is located between the motor and one of the planetary gears of the differential, where the remaining planetary gear is attached to a brake. The satellite gears of the differential gearbox make up the output shaft of the actuator.

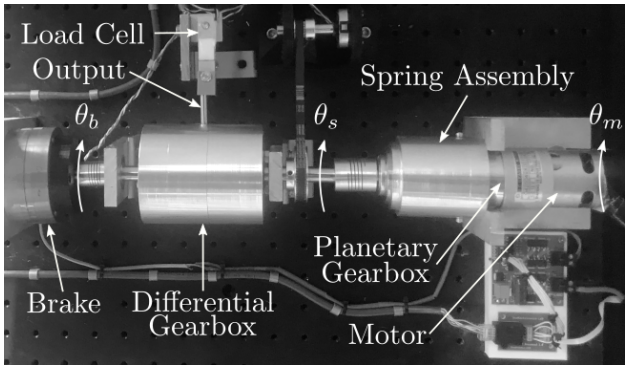

Fig. 2. Image of the multi-input elastic actuator showing the two inputs (motor and brake) as well as the differential clutch mechanism from [3].

backlash, are unified into a single weighted and tunable observed state variable. The controller has a 10 tunable gains, thus its performance and robustness can be adjusted by tuning the feedback controller and observer gains.

The paper is organized as follows. First, the dynamic model of a dual input SEA is presented based on past work presented in [3]. The model is then expanded in Section III to account for backlash affecting the elastic element using Nordin's model [17]. A multi-input active disturbance rejection controller is then formulated in Section IV and the validity of the proposed unified torque controller is verified experimentally and compared to an ADRC controller without backlash compensation and with a classical proportional-integral derivative controller.

II. MIMO Series Elastic Actuator Modelling

Advanced elastic actuators make use of two or more controllable parameters in order to improve performance. To this end, an actuator can be designed to encompass many possible operating modalities throughout strategic use of the controllable elements [1]. As an example, and in order to validate the control approach for MIMO-SEAs proposed in the paper, consider the differentially-clutched SEA we introduced in [3]. The actuator combines a DC motor with a spring, connected to a magnetic particle brake through a differential clutch. A simplified dynamics diagram and image of the device are shown in Fig. 1 and Fig. 2, respectively. The actuator is designed to reproduce the operation of a classical series elastic actuator as well as other operating modes through the use of the clutch. It offers the following operating modes: **Classic SEA mode**: The brake is fully engaged and the actuator reproduces the behaviour of a classical SEA. The motor changes the output torque through the spring. **Elastic mode**: The brake is engaged and the motor is static. The user is then directly coupled to a grounded spring whose stored energy is controlled by adjusting the braking torque. **Hybrid mode**: Both the motor and brake are engaged, thus the brake and differential act as a continuously variable-slip clutch between the spring and the output. As the motor compresses the spring, the brake regulates the amount of energy stored in the spring, thereby controlling the output torque.

The actuator demonstrated above is a multi-input device that measures spring deflection to infer the output torque at the end-effector. The deflection is measured through the difference in encoder measurements between the motor-mounted encoder and the spring-side shaft.

The device dynamics can be summarized by the following set of differential equations [3]:

$$J_m\ddot{\theta}_m + b_m\dot{\theta}_m + k_s\Delta\theta_s = \tau_m \tag{1}$$

$$J_u\ddot{\theta}_u + 4b_d\dot{\theta}_u - 4b_d\dot{\theta}_b - 2k_s\Delta\theta_s = \tau_{out} \tag{2}$$

$$J_b\ddot{\theta}_b - 4b_d\dot{\theta}_u + (4b_d + b_b)\dot{\theta}_b + k_s\Delta\theta_s = \tau_b \tag{3}$$

where k_s is the stiffness of the spring, θ is the angular position, the dot operator $\dot{(\cdot)}$ represents the first time derivative. J and b represent the inertial and viscous friction coefficients. Throughout this paper, subscripts m, b, u, and d represent the dynamics in the motor body, brake body, user/output body, and the differential gearbox, respectively. τ_m is the motor torque, which for low speed can also be related through the input voltage V_m of the device $\tau_m = (K_m V_m)/R_a$ where K_m is the motor torque constant and R_a is the winding resistance of the motor. The brake torque τ_b can be modelled as $\tau_b = f(V_b/R_b)$ where V_b is the voltage input of the brake and R_b is the winding resistance. This function in a natural state is nonlinear due to magnetic hysteresis of the particle brake, however, in this paper it will be simplified to be proportional to the input current through a gain K_h.

The multi-input state space model of the actuator is:

$$\dot{\Theta} = \mathbf{A}\Theta + \mathbf{B}\mathbf{V} \tag{4}$$

where the state input matrices are:

$$\dot{\Theta} = \begin{bmatrix}\dot{\theta}_m & \ddot{\theta}_m & \dot{\theta}_b & \ddot{\theta}_b & \dot{\theta}_s & \ddot{\theta}_s\end{bmatrix}^T$$

$$\mathbf{A} = \begin{bmatrix} 0 & 1 & 0 & 0 & 0 & 0 \\ -\frac{k_s}{J_m} & -\frac{b_m}{J_m} & 0 & 0 & \frac{k_s}{J_m} & 0 \\ 0 & 0 & 0 & 1 & 0 & 0 \\ -\frac{J_u k_s}{J} & 0 & 0 & a_{44} & \frac{J_u k_s}{J} & a_{46} \\ 0 & 0 & 0 & 0 & 0 & 1 \\ \frac{(4J_b - J_u)k_S}{J} & 0 & 0 & a_{64} & \frac{(J_u - 4J_b)k_s}{J} & a_{66} \end{bmatrix}$$

$$\mathbf{B} = \begin{bmatrix} 0 & \frac{K_m}{J_m R_a} & 0 & 0 & 0 & 0 \\ 0 & 0 & 0 & \frac{K_h(J_u - 4J_s)}{R_b J} & 0 & -\frac{K_h J_u}{R_b J} \end{bmatrix}^T, \quad \mathbf{V} = \begin{bmatrix} V_m \\ V_b \end{bmatrix}.$$

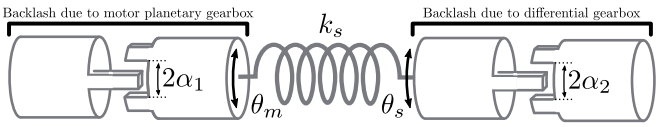

Fig. 3. Backlash on either side of the elastic element in a SEA. The left side represents backlash due to a planetary gearbox in a traditional DC motor, and the right side represents a secondary gearbox in series with the spring transmission. The backlash angle is: $\hat{\theta}_{bk} \in [-(\alpha_1+\alpha_2),(\alpha_1+\alpha_2)]$.

$$
\begin{aligned}
a_{44} &= (J_u(2b_d+b_b) - J_s(4b_d+4b_b-b_u))/J \\
a_{46} &= (J_s(4b_d+b_u) - J_u(b_s+2b_d))/J \\
a_{64} &= (J_b(4b_d+b_u) - J_u(2b_d+b_b))/J \\
a_{66} &= (J_s(b_s+2b_d) + J_b(b_u+4b_s-4b_b))/J \\
J &= 4J_sJ_b - J_uJ_s - J_uJ_b
\end{aligned}
$$

with $\mathbf{V} = \begin{bmatrix} V_m & V_b \end{bmatrix}^T$ as the input vector. When the actuator rotates, the output torque can be calculated based on the relative compression of both sides of the elastic element $\Delta\theta_s$, its stiffness constant $k_s(\Delta\theta_s)$, and all dynamic losses as:

$$\tau_{out} = J_u\ddot{\theta}_u + 4b_d\dot{\theta}_u - 4b_d\dot{\theta}_b - 2k_s\Delta\theta_s \tag{5}$$

where $\Delta\theta_s = \theta_m - \theta_s - \hat{\theta}_{bk}$, and $\hat{\theta}_{bk}$ is the backlash angle affecting the spring deflection $\Delta\theta_s$. The estimation of the backlash angle $\hat{\theta}_{bk}$ is described in the next section.

III. Backlash Estimation and Compensation

The total measured deflection of the elastic element is composed of two primary components that need to be differentiated from one another. The first is the physical deflection in the spring, and the second deals with mechanical backlash, θ_{bk}, which is the positional error due to backlash of the planetary reduction in the motor and the differential gearbox. Thankfully, this can be compensated for based on the actuator dynamic model. This is particularly useful in scenarios in which the nonlinear backlash effect occurs on both sides of the elastic element in the actuator.

Fig. 3 demonstrates the possible sources of mechanical backlash on either side of the elastic element. From the figure, the sum of the backlash from either side of the spring can be defined as $\theta_{bk} = 2\alpha_1 + 2\alpha_2$. The elastic properties of the actuator can be used to provide an insightful estimation of the true deflection of the spring. However, this requires the backlash on either side of the elastic actuator to be measured a priori. If there is compression or expansion in the spring, the elasticity will force the backlash to one of two edges of the transmission system assuming that the spring has a sufficient elastic coefficient, which is generally the case for SEA that deal with power transmission. With this information, estimates of where the true position of the spring shaft is within the range of the backlash. If deflection in the spring occurs, there exists a torque experienced at the output and, therefore, backlash can be estimated using Nordin's exact model [17] as follows:

$$
\hat{\theta}_{bk} = \begin{cases} \max\left(0, \dot{\theta}_m - \dot{\theta}_s + \frac{k_s}{b_m}(\theta_m - \theta_s - \theta_{bk})\right) & \text{if } \tau_s < 0 \\ \dot{\theta}_m - \dot{\theta}_s + \frac{k_s}{b_m}(\theta_m - \theta_s - \theta_{bk}) & \text{if } \tau_s = 0 \\ \min\left(0, \dot{\theta}_m - \dot{\theta}_s + \frac{k_s}{b_m}(\theta_m - \theta_s - \theta_{bk})\right) & \text{if } \tau_s > 0 \end{cases} \tag{6}
$$

Estimating backlash grants a metric in which the torque can be controlled based on measurements of spring deflection. However, since the deflection angle is used to compute torque, the condition for $\tau_s > 0$ rad is only certain when $\theta_m - \theta_s > \theta_{bk}$. Or conversely, $\tau_s < 0 \iff (\theta_m - \theta_s) < \theta_{bk}$. Alternatively, the conditions can be met when the estimated backlash angle has reached the limits $\hat{\theta}_{bk} = -(\alpha_1+\alpha_2) \implies \tau_s < 0$ or $\hat{\theta}_{bk} = (\alpha_1+\alpha_2) \implies \tau_s > 0$.

IV. Multi-Input Active Disturbance Rejection Torque Controller

The objective of ADRC is to provide accurate torque outputs based strictly on measurements of the deflection of the spring. With the estimate of the backlash angle, a reasonable estimate of the true deflection angle can be extracted from the encoder readings on either side of the spring. Backlash can then be compensated for and the updated reference can be used to compute error in the controller. Active disturbance rejection control (ADRC) will be used for this purpose, as ADRC is an error-based control method that can be used to compensate for backlash via a transient profile generator, i.e., a time-optimal solution reference trajectory designed for non-ideal systems. The output of the controller can be distributed to multiple inputs, which is the case for the actuator described by (4). Convergence of nonlinear ADRC for multi-input systems is demonstrated in [23].

A. Reference and Transient Output Torque Profile

The proportional and time varying error, e_1 and e_2, respectively, with backlash compensation can be calculated as:

$$e_1(k) = \tau_{ref}(k) - \tau_{inf}(k) = \tau_{ref} - k_s(\theta_m - \theta_s - \theta_{bk}) \tag{7}$$

$$e_2(k) = e_2(k-1) + h\ fhan(e_1(k), e_2(k-1), r_0, h_0) \tag{8}$$

where τ_{ref} is the reference torque, τ_{inf} is the inferred output torque measured from the deflection of the elastic element, and θ_{bk} is defined in (6). These errors can be inserted into the *fhan* function from [24] along with the acceleration rate r_0 and smoothing factor h_0 to produce a *desired transient profile* as shown in Fig. 4. The *fhan* function can be described as:

$$fhan(e_1, e_2, r_0, h_0) = -r_0\left[\left(\frac{a}{h_0 r_0^2} - \text{sign(a)}\right)s_a + \text{sign}(a)\right] \tag{9}$$

The above function creates the reference transient profiles demonstrated in Fig. 4. The figure demonstrates four transient profiles with differing acceleration rates r_0 to a proposed reference spring deflection. The constants used in (9) are:

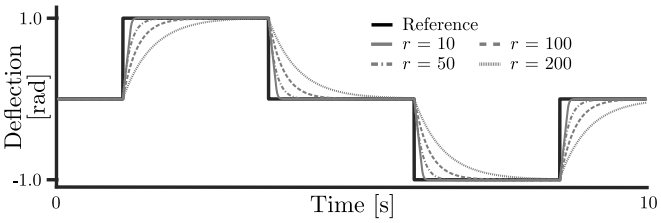

Fig. 4. Transient profiles generated with various acceleration rates $r = 10, 50, 100, 200$ for a reference deflection signal. The transient profile for desired spring deflection provides an achievable alternative reference signal compared to the infinite derivative reference square profile.

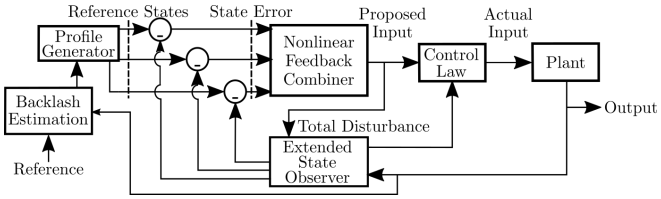

Fig. 5. Block diagram of a simplified version of the controller. The profile generator adjusts the input at unrealistic instantaneous reference shifting to improve differential tracking error; the nonlinear feedback combiner aggregates the proportional and differential error in the states and proposes an input to the plant. The extended state observer provides a means of estimating and compensating unmodeled disturbances by creating a new state that encapsulates all disturbances in the system.

$$
\begin{aligned}
s_a &= \text{sign}(a + h_0 r_0^2)/2 - \text{sign}(a - h_0 r_0^2)/2 \\
s_y &= \text{sign}(e_1 + h_0 e_2 + h_0 r_0^2) - \text{sign}(e_1 + h_0 e_2 - h_0 r_0^2)/2 \\
a_2 &= h_0 e_2 + \text{sign}(e_1 + h_0 e_2)(a_1 - h_0 r_0^2)/2 \\
a_1 &= \sqrt{h_0 r_0^2 \left(h_0 r_0^2 + 8|e_1 + h_0 e_2|\right)} \\
a &= (h_0 e_2 + e_1 + h_0 e_2 - a_2) s_y + a_2
\end{aligned}
$$

The reference functions obtained from *fhan* produce a realistic alternative to transients in physical systems, as an input reference such as a heaviside step has an infinite derivative at the transient point which is impossible to recreate.

Consider the MISO time varying system described in Section II with six measured states variables defined by the vector $\Theta^i \in \mathbb{R}$, $i = 1,2,3$ as $\Theta = [x_1^1 \quad x_2^1 \quad x_1^2 \quad x_2^2 \quad x_1^3 \quad x_2^3]^T = [\theta_m \quad \dot{\theta}_m \quad \theta_s \quad \dot{\theta}_s \quad \theta_b \quad \dot{\theta}_b]^T$. A block diagram of the controller is shown in Fig. 5. In this example, a system with three independent states θ_m, θ_s, and θ_b as well as their first time derivatives are measurable. Therefore, a total of three system equations for the ADRC controller can be utilized. Each of the three subsystems ($i = 1,2,3$) and their respective nonlinearities can be described using the following set of equations:

$$
\begin{cases}
\dot{x}_1^i = f_1^i(t, x_1^1, x_2^1, x_1^2, x_2^2, x_1^3, x_2^3, D^i(t)) \\
\dot{x}_2^i = f_2^i(t, x_1^1, x_2^1, x_1^2, x_2^2, x_1^3, x_2^3, D^i(t)) \\
\qquad\qquad + b^i(t, x_1^1, x_2^1, x_1^2, x_2^2, x_1^3, x_2^3)u \\
y^i = x_1^i,
\end{cases} \tag{10}
$$

where $f_j, j = 1,2$ and b are imperfect or nonlinear functions describing the subsystem and any external disturbances experienced by the subsystem $D(t)$. $u^i(t)$ is the control input of the subsystem, and $y^i(t)$ is the output, an angular displacement for the multi-input plant described in Section II. The three local total disturbance terms can be estimated and combined by equating $\bar{x}_1^i = y^i$ and $\bar{x}_2^i = f_1^i(t, x_1^1, x_2^1, x_1^2, x_2^2, x_1^3, x_2^3, D^i(t))$, which provides the following description of the subsystem with a common disturbance:

$$
\begin{cases}
\dot{\bar{x}}_1^i = \bar{x}_2^i \\
\dot{\bar{x}}_2^i = \frac{\partial \bar{x}_2^i}{\partial t} + \frac{\partial \bar{x}_2^i}{\partial x_1^1}\frac{\partial x_1^1}{\partial t} + \frac{\partial \bar{x}_2^i}{\partial x_2^1}\frac{\partial x_2^1}{\partial t} + \frac{\partial \bar{x}_2^i}{\partial x_1^2}\frac{\partial x_1^2}{\partial t} + \frac{\partial \bar{x}_2^i}{\partial x_2^2}\frac{\partial x_2^2}{\partial t} \\
\qquad + \frac{\partial \bar{x}_2^i}{\partial x_1^3}\frac{\partial x_1^3}{\partial t} + \frac{\partial \bar{x}_2^i}{\partial x_2^3}\frac{\partial x_2^3}{\partial t} + \frac{\partial \bar{x}_2^i}{\partial D^i}\frac{\partial D^i}{\partial t} - \frac{\partial \bar{x}_2^i}{\partial x_2^i}\frac{\partial x_2^i}{\partial t} \\
\qquad\qquad + \frac{\partial \bar{x}_2^i}{\partial x_2^i} f_2^i(t, x_1^1, x_2^1, x_1^2, x_2^2, x_1^3, x_2^3, D^i(t)) \\
\qquad\qquad\qquad + \frac{\partial \bar{x}_2^i}{\partial x_2^i} b^i(t, x_1^1, x_2^1, x_1^2, x_2^2, x_1^3, x_2^3) u^i(t) \\
y^i = \bar{x}_1^i
\end{cases} \tag{11}
$$

A linear approximation $\bar{b}^i(t)$ for the nonlinear term b^i allows the subsystem to be extended by a new state representing the sum of disturbance as $\bar{x}_3^i$. This disturbance and its first time derivative $\dot{\bar{x}}_3^i$ is defined by:

$$
\begin{cases}
\dot{\bar{x}}_2^i = \bar{x}_3^i + \bar{b}^i(t) u^i(t) \\
\dot{\bar{x}}_3^i = f_3^i(t, x_1^1, x_2^1, x_1^2, x_2^2, x_1^3, x_2^3)
\end{cases} \tag{12}
$$

where the total disturbance can be combined as:

$$
\begin{aligned}
\bar{x}_3^i = &\frac{\partial \bar{x}_2^i}{\partial t} + \frac{\partial \bar{x}_2^i}{\partial x_1^1}\frac{\partial x_1^1}{\partial t} + \frac{\partial \bar{x}_2^i}{\partial x_2^1}\frac{\partial x_2^1}{\partial t} + \frac{\partial \bar{x}_2^i}{\partial x_1^2}\frac{\partial x_1^2}{\partial t} + \frac{\partial \bar{x}_2^i}{\partial x_2^2}\frac{\partial x_2^2}{\partial t} \\
&+ \frac{\partial \bar{x}_2^i}{\partial x_1^3}\frac{\partial x_1^3}{\partial t} + \frac{\partial \bar{x}_2^i}{\partial x_2^3}\frac{\partial x_2^3}{\partial t} + \frac{\partial \bar{x}_2^i}{\partial D^i}\frac{\partial D^i}{\partial t} - \frac{\partial \bar{x}_2^i}{\partial x_2^i}\frac{\partial x_2^i}{\partial t} \\
&+ \frac{\partial \bar{x}_2^i}{\partial x_2^i} f_2^i(t, x_1^1, x_2^1, x_1^2, x_2^2, x_1^3, x_2^3, D^i(t)) \\
&+ \left(\frac{\partial \bar{x}_2^i}{\partial x_2^i} b^i(t, x_1^1, x_2^1, x_1^2, x_2^2, x_1^3, x_2^3) - \bar{b}^i(t) \right) u^i(t)
\end{aligned} \tag{13}
$$

The controller utilizes three extended state observers (ESO) to measure the angular displacement and velocity of each of the subsystems. The ESO can be used to evaluate discrepancies in expected values and, therefore, estimate disturbances in each of the subsystems. The state extension of the ESO provides a means of evaluating nonlinearities around the spring deflection, magnetic hysteresis, static friction, and other unmodelled disturbances. Each of the three extended state observers can be defined as:

$$
\begin{cases}
\dot{\hat{x}}_1^i = \hat{x}_2^i - \beta_{01}^i g_1^i(\theta_m, \theta_b, \theta_s, \theta_{bk}, \hat{y}^i(t)) \\
\dot{\hat{x}}_2^i = \hat{x}_3^i - \beta_{02}^i g_2^i(\theta_m, \theta_b, \theta_s, \theta_{bk}, \hat{y}^i(t)) + \bar{b}^i u(t) \\
\dot{\hat{x}}_3^i = -\beta_{03}^i g_3^i(\theta_m, \theta_b, \theta_s, \theta_{bk}, \hat{y}^i(t)) \\
\hat{y}^i = \hat{x}_1^i,
\end{cases} \tag{14}
$$

where $\beta_{0j}^i \quad j = 1,2,3$ are the observer gains for a dual integral plant state i and $g(\theta_m, \theta_b, \theta_s, \theta_{bk}, \hat{y}(t))$ are chosen error functions considering the actuator backlash in (6). This allows the ADR control law to be written as:

$$
u^i(t) = -(\hat{x}_{n+1}^i(t) - u_0^i)(\bar{b}^i)^{-1} \tag{15}
$$

where u_0^i is a potential control input from a weighted

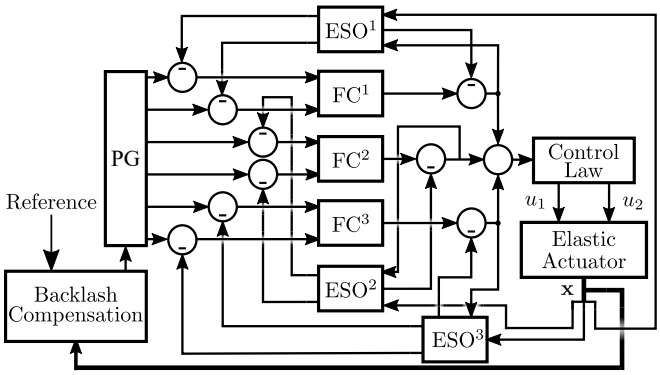

Fig. 6. Overall updated nonlinear backlash compensated ADRC scheme for a multi-input SEA. Three feedback combiners (FC) and three extended state observers (ESO) are utilized to adapt to perturbations in the spring deflection. The reference is first input into the backlash compensator, where an updated profile is implemented through the transient profile generator (PG). The estimated states from the ESO are then combined into NFC and finally distributed through the control law.

feedback combiner:

$$u_0^i = k_1^i(v - \hat{x}_1^i) + k_2^i(\dot{v} - \hat{x}_2^i), \tag{16}$$

where $v = v^- + h\dot{v}^-$ and $\dot{v} = \dot{v}^- + h \;\; fhan(e_1, e_2^-, r_0, h_0)$ are the adjusted control references by the transient profile generator and $k_1 = 1.25$ and $k_2 = 2$ are tunable gains to achieve a desired performance.

B. Control Law

There are two primary methods of handling the MISO system for inferred torque control. The first way of controlling the actuator, similar to a traditional series elastic actuator, is by fully engaging the brake and exclusively using the motor to control the spring deflection. This can reduce the number of controllable inputs to one and, therefore, reduce the number of feasible solutions to obtaining a reference deflection. In this case, the control input is simply:

$$V_m = u_0 = -\left.\frac{fhan(e_1, ce_2, h_1, r_1) - \hat{x}_3}{\bar{b}}\right| \tau_{cb} > \tau_{out} + \tau_s, \tag{17}$$

where e_1 and e_2 are the observed proportional and time-varying error values defined in (7) and (8), c is a fine tuning parameter related to the differential reference, and z_3 is the total disturbance estimated by the observer. In plants containing multiple inputs working to achieve a common goal, multiple solutions exist for producing a reference torque and, therefore, a multi-input controller must be used.

A second method makes use of both controllable inputs in a distributive manner. The proposed input of the rejection controller can be distributed between the motor voltage V_m and brake voltage V_b, the two control inputs are:

$$u_0 = f_1(k_s\Delta\theta_s)V_m^{max} + f_2(k_s\Delta\theta_s)V_b^{max} \tag{18}$$

$$= -\sum_{i=1}^{3} \frac{p_0^i(fhan(e_1^i, c^i e_2^i, h_1^i, r_1^i) - \hat{x}_3^i)}{\bar{b}^i}, \tag{19}$$

TABLE I
ACTIVE DISTURBANCE REJECTION TUNED PARAMETERS.

Gain	T_s	h_0	r_0	c	b_0	β_{01}	β_{02}	β_{03}
Value	0.002	0.002	50	1	0.1	1	167	7813

where:

$$\forall k_s\Delta\theta_s < \tau_{ref} \exists [f_1(k_s\Delta\theta_s) > 0] \wedge [f_2(k_s\Delta\theta_s) > 0] \ni \Delta\dot{\theta}_s \geq 0. \tag{20}$$

and:

$$\forall k_s\Delta\theta_s > \tau_{ref} \exists [f_1(k_s\Delta\theta_s) < 0 \wedge f_2(k_s\Delta\theta_s) > 0] \vee [f_1(k_s\Delta\theta_s) = 0 \wedge f_2(k_s\Delta\theta_s)] = u_0/V_b) \ni \Delta\dot{\theta}_s \leq 0 \tag{21}$$

with $f_1 \in [-1, 1], f_2 \in [0, 1]$ being linear distributing functions dependent on the current state of the spring deflection and the reference torque, and p_0^i is a tuning parameter to produce meaningful distribution of the inputs.

V. EXPERIMENTAL RESULTS

The importance of backlash compensation in elastic actuators becomes more apparent in an experimental setting. Fig. 7 compares three controllers when the multi-input actuator behaves has a single-input device. To this end, the brake is continuously engaged and therefore the device acts as a traditional SEA. The evaluated SISO controllers are:

- Single-input controller 1: An active disturbance rejection controller (ADRC) without backlash compensation;
- Single-input controller 2: A backlash-compensated active disturbance rejection controller;
- Single-input controller 3: A proportional-integral-derivative (PID) controller as a basis of comparison.

The tuned parameters for all ADR controllers used are provided in Table I. The actuator was connected to a static load cell and a reference deflection (pseudo-torque control) was controlled in square pulses of ± 1 rad. Fig. 7(a) shows the performance of the three controllers to a reference deflection.

If backlash is not considered, which is the case for PID and classical ADRC, raw encoder inputs about the deflection are taken to be the true deflection angle of the spring causing deviations in expected output torque ($\Delta\theta_s = \theta_m - \theta_s - \theta_{bk}$). With backlash compensation, an updated estimation of the true deflection can be inferred through the addition of the estimated backlash angle ($\Delta\theta_s = (\theta_m - \theta_s - \theta_{bk}) + \hat{\theta}_{bk}$).

The next experiments were conducted using the multi-input control law (19). The distributive method was applied providing the following evaluated controllers:

- Multi-input controller 1: An active disturbance rejection controller (ADRC) without backlash compensation;
- Multi-input controller 2: A backlash-compensated active disturbance rejection controller;
- Multi-input controller 3: PID controller single output distributed as $V_b = 0.7u_0$ and $V_m = 0.3u_0$;

Fig. 8(a) demonstrates a similar experiment utilizing both inputs of the series elastic actuator. The raw measured deflection of the backlash compensated ADRC does not follow the reference trajectory as closely as the classical controllers

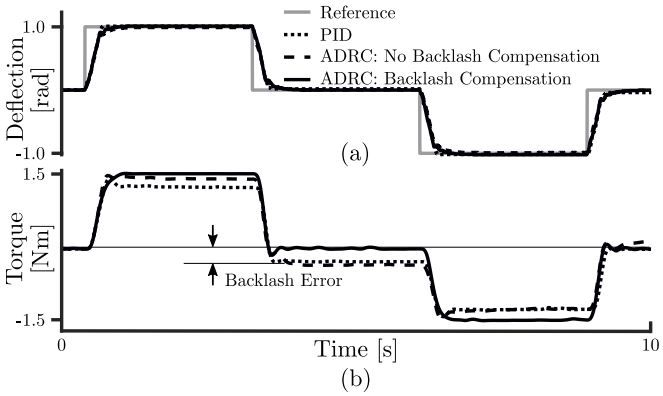

Fig. 7. Results of single-input deflection control with PID, classical ADRC, and backlash compensated ADRC. Note that measured deflection in each of the three compared control schemes are similar, however, each produces different torque profiles at the output, rendering different results for the same measured parameters.

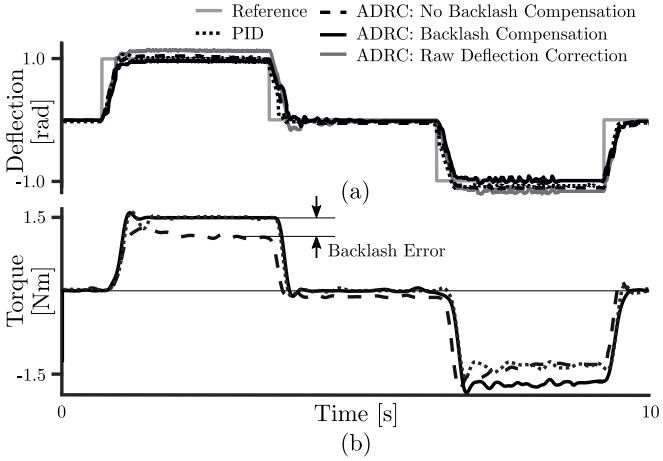

Fig. 8. Results of multi-input control on the spring deflection to reference square pulses. The backlash compensated ADRC has updated reference deflection profile to compensate for nonlinearities in the spring.

to compensate for uncertainties in the actuator backlash. This provides an output torque with better symmetry that is not dependent on the initial conditions (θ_{bk} at $t = 0$). The effects of backlash compensation are most apparent at low torques and in the transition from positive to negative reference deflections. Fig. 9(a) demonstrates a scenario in which the desired spring deflection continuously transitions from 1 rad to -1 rad. Similar to previous experiments, each of the three compared controllers were able to maintain the desired deflection, however, only the backlash compensated controller generates an estimate of the backlash angle $\hat{\theta}_{bk}$ as shown in Fig. 9(b). Fig. 9(c) demonstrates the externally measured output torque for all three controllers and compares the output torque to an ideal linear spring. As shown, the controllers without backlash compensation were influenced by the nonlinearity in the spring and the zero-torque deadzone caused by actuator backlash. In the controller with backlash compensation, the torque relates closer to the ideal linear spring and has a minimal deadzone. Total error from an ideal linear output for each controller is displayed in Fig. 9(d).

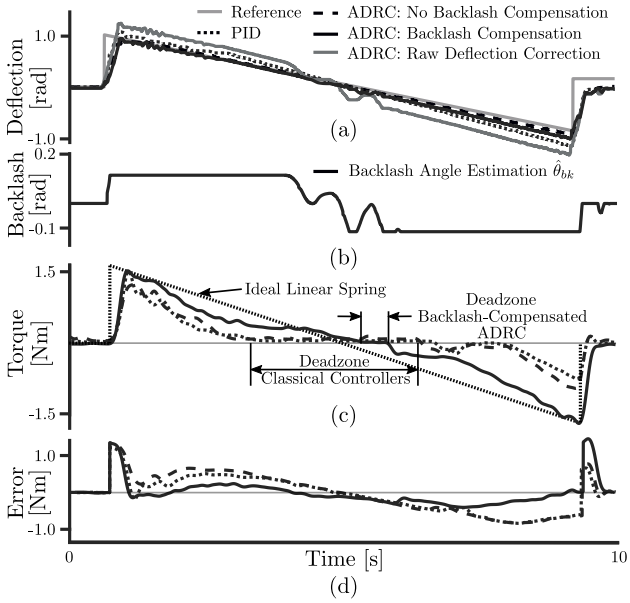

Fig. 9. Demonstration of nonlinearities in spring through multi-input sawtooth deflection control. (a) shows the deflection control using PID, classical ADRC, as well as backlash-compensated ADRC. The backlash-compensated ADRC demonstrates the corrected true deflection angle ($\theta_m - \theta_s$) as well as the raw measured angle ($\theta_m - \theta_s - \hat{\theta}_{bk}$). (b) shows the estimated backlash angle $\hat{\theta}_{bk}$. (c) Demonstrates the measured output torque compared to an ideal linear spring and a system with no backlash. Zero-torque deadzones are also highlighted as an effect of actuator nonlinearities. (d) shows the error between the measured torques for each controller and an ideal spring.

VI. Conclusions

Torque estimation and resolution are important metrics to evaluate the performance of SEAs. Active disturbance rejection is an attractive control method for SEAs as it is able to handle nonlinear effects as well as unmodelled disturbances. SEAs tend to be largely nonlinear and, therefore, ADRC provides the advantages of using an error based control method without having a perfect model of the plant.

However, the nonlinearities around deflection of the spring can cause unwanted behavior since deflection is often the controlled parameter in SEAs. It is difficult to determine the exact output torque of SEAs without the use of external sensing devices and, therefore, an ideal SEA would have a linear relationship between the measured spring deflection and the output torque. To this end, mechanical backlash can have adverse effects on the performance of a SEA if it is desirable to operate the actuator without a torque sensor.

The proposed unified backlash-compensated multi-input ADRC is a robust method to reduce the effect of nonlinearities caused by mechanical backlash and spring deflection. The updated reference deflection allows the output torque to follow a desired trajectory with less error caused from directional changes or low torques, improving the torque bandwidth of the actuator. Backlash compensation also ensures the measured deflection in the spring is as accurate and symmetric as possible. Compensating for this nonlinearity is easily implementable and produced consistent results as compared to classical error-based control methods.

REFERENCES

[1] G. A. Pratt and M. M. Williamson, "Series elastic actuators," in *Proceedings 1995 IEEE/RSJ International Conference on Intelligent Robots and Systems. Human Robot Interaction and Cooperative Robots*, vol. 1. IEEE, 1995, pp. 399–406.

[2] A. Calanca and P. Fiorini, "Human-adaptive control of series elastic actuators," *Robotica*, vol. 32, no. 8, pp. 1301–1316, 2014.

[3] B. DeBoon, S. Nokleby, N. La Delfa, and C. Rossa, "Differentially-clutched series elastic actuator for robot-aided musculoskeletal rehabilitation," in *2019 International Conference on Robotics and Automation (ICRA)*. IEEE, 2019, pp. 1507–1513.

[4] K. Kong, J. Bae, and M. Tomizuka, "Control of rotary series elastic actuator for ideal force-mode actuation in human–robot interaction applications," *IEEE/ASME Transactions on Mechatronics*, vol. 14, no. 1, pp. 105–118, 2009.

[5] G. Smoljkic, G. Borghesan, D. Reynaerts, J. De Schutter, J. Vander Sloten, and E. Vander Poorten, "Constraint-based interaction control of robots featuring large compliance and deformation," *IEEE Transactions on Robotics*, vol. 31, no. 5, pp. 1252–1260, 2015.

[6] Y. She, D. Meng, J. Cui, and H.-J. Su, "On the impact force of human-robot interaction: Joint compliance vs. link compliance," in *2017 IEEE International Conference on Robotics and Automation (ICRA)*. IEEE, 2017, pp. 6718–6723.

[7] J. Kim, A. Alspach, and K. Yamane, "3d printed soft skin for safe human-robot interaction," in *2015 IEEE/RSJ International Conference on Intelligent Robots and Systems (IROS)*. IEEE, 2015, pp. 2419–2425.

[8] M. Safeea and P. Neto, "Minimum distance calculation using laser scanner and imus for safe human-robot interaction," *Robotics and Computer-Integrated Manufacturing*, vol. 58, pp. 33–42, 2019.

[9] P. Neto, M. Simão, N. Mendes, and M. Safeea, "Gesture-based human-robot interaction for human assistance in manufacturing," *The International Journal of Advanced Manufacturing Technology*, vol. 101, no. 1-4, pp. 119–135, 2019.

[10] F. Conti and O. Khatib, "A new actuation approach for haptic interface design," *The International Journal of Robotics Research*, vol. 28, no. 6, pp. 834–848, 2009.

[11] B. Chen, X. Zhao, H. Ma, L. Qin, and W.-H. Liao, "Design and characterization of a magneto-rheological series elastic actuator for a lower extremity exoskeleton," *Smart Materials and Structures*, vol. 26, no. 10, p. 105008, 2017.

[12] E. J. Rouse, L. M. Mooney, and H. M. Herr, "Clutchable series-elastic actuator: Implications for prosthetic knee design," *The International Journal of Robotics Research*, vol. 33, no. 13, pp. 1611–1625, 2014.

[13] T. Zhang and H. Huang, "Design and control of a series elastic actuator with clutch for hip exoskeleton for precise assistive magnitude and timing control and improved mechanical safety," *IEEE/ASME Transactions on Mechatronics*, 2019.

[14] C. Rossa, J. Lozada, and A. Micaelli, "Design and control of a dual unidirectional brake hybrid actuation system for haptic devices," *IEEE Transactions on Haptics*, vol. 7, no. 4, pp. 442–453, 2014.

[15] A. Tustin, "The effects of backlash and of speed-dependent friction on the stability of closed-cycle control systems," *Journal of the Institution of Electrical Engineers-Part IIA: Automatic Regulators and Servo Mechanisms*, vol. 94, no. 1, pp. 143–151, 1947.

[16] Z. Shi and Z. Zuo, "Backstepping control for gear transmission servo systems with backlash nonlinearity," *IEEE Transactions on Automation Science and Engineering*, vol. 12, no. 2, pp. 752–757, 2014.

[17] M. Nordin, J. Galic', and P.-O. Gutman, "New models for backlash and gear play," *International Journal of Adaptive Control and Signal Processing*, vol. 11, no. 1, pp. 49–63, 1997.

[18] M. Nordin and P.-O. Gutman, "Controlling mechanical systems with backlash-a survey," *Automatica*, vol. 38, no. 10, pp. 1633–1649, 2002.

[19] S. Oh and K. Kong, "High-precision robust force control of a series elastic actuator," *IEEE/ASME Transactions on Mechatronics*, vol. 22, no. 1, pp. 71–80, 2016.

[20] E. Sariyildiz, G. Chen, and H. Yu, "A unified robust motion controller design for series elastic actuators," *IEEE/ASME Transactions on Mechatronics*, vol. 22, no. 5, pp. 2229–2240, 2017.

[21] X. Yang, J. Cui, D. Lao, D. Li, and J. Chen, "Input shaping enhanced active disturbance rejection control for a twin rotor multi-input multi-output system (trms)," *ISA Transactions*, vol. 62, pp. 287–298, 2016.

[22] J. Pratt, B. Krupp, and C. Morse, "Series elastic actuators for high fidelity force control," *Industrial Robot: An International Journal*, vol. 29, no. 3, pp. 234–241, 2002.

[23] B.-Z. Guo and Z.-L. Zhao, "On convergence of the nonlinear active disturbance rejection control for mimo systems," *SIAM Journal on Control and Optimization*, vol. 51, no. 2, pp. 1727–1757, 2013.

[24] J. Han, "From pid to active disturbance rejection control," *IEEE Transactions on Industrial Electronics*, vol. 56, no. 3, pp. 900–906, 2009.